The spatial heterogeneity of cloud phase observed by satellite

Adam B. Sokol[1], **Trude Storelvmo**[2]

[1]Department of Atmospheric Sciences, University of Washington, Seattle, WA, USA

[2]Department of Geosciences, University of Oslo, Oslo, Norway,

Key Points:

- Cloud phase heterogeneity observed by lidar is greatest a few degrees below freezing, when single-phase patches are 6 km in length on average
- Heterogeneity is greatest in the northern mid-latitudes and relatively low over the Southern Ocean
- Extratropical heterogeneity undergoes an annual cycle that reflects seasonal shifts in the storm track

Corresponding author: Adam B. Sokol, abs66@uw.edu

Abstract

We conduct a global assessment of the spatial heterogeneity of cloud phase within the temperature range where liquid and ice can coexist. Single-shot CALIOP lidar retrievals are used to examine cloud phase at the 333-m scale, and heterogeneity is quantified according to the frequency of switches between liquid and ice along the satellite's path. In the global mean, heterogeneity is greatest from -15 to -2°C with a peak at -4°C, when small patches of ice are prevalent within liquid-dominated clouds. Above -20°C, heterogeneity is greatest in the northern midlatitudes and lower over the Southern Ocean, where supercooled liquid clouds dominate. Zonal mean heterogeneity undergoes an annual cycle with a peak that follows seasonal shifts in the extratropical storm track. These results can be used to improve the representation of subgrid-scale heterogeneity in general circulation models, which has the potential to reduce model biases in phase partitioning and radiation balance.

Plain Language Summary

At temperatures where ice and liquid can coexist within clouds, climate models produce too much ice and too little liquid compared to satellite observations. This bias is caused by the assumption that liquid and ice are uniformly mixed, which results in the rapid conversion of liquid to ice for thermodynamic reasons. To reduce this bias, models need to account for the spatial heterogeneity ("patchiness") of liquid and ice that exists in the real atmosphere. The goal of this paper is to quantify this spatial heterogeneity using satellite observations of cloud phase. To do so, we use vertical profiles of cloud phase observed by the CALIOP lidar every 333 m along the satellite's path. Clouds with small alternating pockets of liquid and ice are said to be more heterogeneous. We find small pockets of ice in liquid-dominated clouds to be more common than small pockets of liquid in ice-dominated clouds. The greatest heterogeneity is found in the northern midlatitudes and follows seasonal shifts in storminess. Phase is relatively homogeneous over the Southern Ocean, where supercooled liquid clouds dominate. These results can be used in the future to improve model representations of the thermodynamic processes responsible for biases in cloud phase.

1 Introduction

Cloud feedbacks remain a leading source of uncertainty in estimates of climate sensitivity (Zelinka et al., 2020). One such feedback is the cloud phase feedback, which was first described by Mitchell et al. (1989) as a negative feedback resulting from a shift in cloud phase partitioning from ice to liquid with warming. The feedback is negative because liquid cloud droplets are generally smaller and more numerous than ice crystals, which means that liquid clouds are optically thicker than ice clouds of equal condensate mass. A shift in phase partitioning from ice to liquid therefore produces an increase in cloud albedo.

The magnitude of the cloud phase feedback has proved tricky to constrain using models, largely because of its sensitivity to the phase partitioning of the initial state (Storelvmo et al., 2015; Choi et al., 2014; Tsushima et al., 2006). General circulation models (GCMs) systematically produce too much ice and too little liquid within the mixed-phase temperature range (-40 to 0°), especially over the Southern Ocean (Cesana et al., 2015; Komurcu et al., 2014; Kay et al., 2016). As a result, present-day cloud albedo is too low in many GCM simulations, and the albedo enhancement associated with ice-to-liquid transitions is too dramatic. Adjustment of present-day phase partitioning to more closely match observations results in a weakened cloud phase feedback and an increase in simulated climate sensitivity (Tan et al., 2016; Frey & Kay, 2018)

Model biases in phase partitioning are thought to be caused, at least in part, by an overactive Wegener-Bergeron-Findeisen (WBF) process (Tan & Storelvmo, 2016; McIlhattan et al., 2017). The WBF process is a consequence of the difference in saturation vapor pressures with respect to liquid and ice, which, in a mixed-phase environment, can cause ice crystals to grow at the expense of nearby liquid droplets (Storelvmo & Tan, 2015). GCM parameterizations of the WBF process typically assume that liquid and ice are homogeneously mixed throughout a model grid box, which allows for efficient WBF glaciation of supercooled liquid. But aircraft observations, while limited, suggest that mixed-phase clouds often contain discrete liquid-only and ice-only pockets much smaller than a GCM grid box (A. V. Korolev et al., 2003; Chylek & Borel, 2004; Field et al., 2004). By reducing the spatial overlap of ice and liquid condensate, this heterogeneity could limit WBF efficiency in the real atmosphere, and previous work has shown that accounting for heterogeneity can mitigate model biases in phase partitioning (Tan & Storelvmo, 2016;

Zhang et al., 2019; Huang et al., 2021). An important takeaway from this previous work is that there is no one-size-fits-all adjustment to WBF efficiency that improves model phase biases across the board: the sensitivity of phase biases to WBF efficiency varies with location, season, and temperature, and this variability presumably reflects different degrees of phase heterogeneity in the real world. Attempts to reduce model phase biases, if they are to be physically grounded, must therefore account not only for the existence of phase heterogeneity but also for its spatial and temporal variability.

Understanding phase heterogeneity in the real atmosphere is a difficult problem because it occurs on scales ranging from microns to kilometers (A. V. Korolev et al., 2003; Atlas et al., 2021). Capturing this range of scales requires in situ aircraft observations, which typically have a measurement frequency of 1 Hz (every 100-200 m, depending on aircraft speed). Studies making use of the measurements have generally shown that a relatively small portion of 1-Hz observations within the mixed-phase temperature range contain both liquid and ice; most are single-phase or heavily dominated by one phase or the other (A. V. Korolev et al., 2003; Field et al., 2004; D'Alessandro et al., 2019; D'Alessandro et al., 2021; Zhang et al., 2019). For example, Zhang et al. (2019) analyzed data from the HIPPO aircraft campaign and found that only 13.4% of 1-Hz observations between -40-0°C were mixed-phase. Even when the data were smoothed by a 100-s (∼20-km) rolling average, only 25.8% were mixed-phase. On the whole, these aircraft studies suggest that mixed-phase conditions at the 100-m scale are relatively rare. This is not surprising given that mixtures of liquid and ice are thermodynamically unstable, which is what gives rise to the WBF process in the first place. Nevertheless, these observational assessments come with considerable uncertainty arising from imperfect phase classification algorithms and varying definitions of "mixed-phase". Perhaps most importantly, aircraft observations are limited in number, and the generalizability of existing observations is unknown.

Spaceborne satellite observations are a largely untapped resource for studying cloud phase heterogeneity. Thompson et al. (2018) assessed cloud-top phase heterogeneity using retrievals from the Hyperion spectrometer, but the spatial coverage of the observations was sparse and included very few measurements of the mid-latitude oceans, where model phase biases are most severe. Moreover, the reliance of the spectrometer retrieval on reflected sunlight meant that observations were limited to daytime hours and only reflected conditions near cloud top. These limitations can be largely overcome by polar-orbiting satellites with active sensors, which offer near-global coverage over extended pe-

riods of time and can penetrate below cloud top until their signal is attenuated. While these satellites cannot capture the fine spatial scales observable by aircraft and Hyperion, the aircraft observations discussed previously suggest that a resolution of a few hundred meters can capture a large portion of cloud phase variability. For these reasons, we believe active-sensing satellites are a promising avenue for understanding phase heterogeneity on a global scale and improving its representation in models.

The goal of this work is to quantify cloud phase heterogeneity and its spatiotemporal variability using spaceborne lidar measurements. The lidar observations are described in section 2. In section 3, we develop a metric that is used to characterize phase heterogeneity in the satellite record. Results are presented in section 4 and 5 and discussed in section 6.

2 Observational Data

Observations of cloud phase were obtained from the Cloud-Aerosol Lidar with Orthogonal Polarization (CALIOP) aboard the polar-orbiting CALIPSO satellite (Winker et al., 2009). The reasons for using CALIOP are its near-global coverage and its relatively high horizontal resolution: single-shot profiles of the atmosphere have a horizontal footprint of 90 m and are recorded every 333 m along the satellite's path.

In the CALIOP retrievals used here (version 4), cloud phase is determined based on the layer-integrated attenuated backscatter and depolarization ratio (Hu et al., 2009; Avery et al., 2020). Each cloudy pixel is classified as liquid, randomly oriented ice, horizontally oriented ice, or unknown. Each phase determination is accompanied by a quality indicator, which we use to eliminate low-confidence determinations. The lack of a mixed-phase classification is a clear limitation of the CALIOP phase retrievals, since mixed-phase conditions are known to occur on length scales much smaller than 333 m (Field et al., 2004; Atlas et al., 2021). Clouds identified as supercooled liquid may contain small amounts of ice that cannot be detected by spaceborne lidar because, in mixed-phase conditions, the number concentration of ice crystals is generally much lower than that of liquid droplets (Mace et al., 2021).

The cloud phase data used here are from CALIOP Level 2 Vertical Feature Mask data product (version 4.20; NASA/LARC/SD/ASDC, 2018b), which provides cloud phase retrievals at the single-shot resolution of 333 m up to an altitude of 8.2 km, above which

the resolution if coarsened due to bandwidth limitations. Because we wish to use the finest resolution possible, we restrict our analysis to levels below 8.2 km. This is not an issue for studying the mid- and high latitudes, where clouds above 8.2 km are almost entirely ice (Cesana et al., 2015). We use all available data for the three-year period between 2009-12-01 and 2012-11-30. This amounts to over 35 billion individual cloud observations, 83% of which have medium- or high-quality phase determinations. Temperature data for the same period are obtained from the CALIOP Level 2 Cloud Profile data product (version 4.20; NASA/LARC/SD/ASDC, 2018a), which provides temperature from the GEOS-5 reanalysis interpolated onto the CALIPSO track with a horizontal resolution of 5 km and a vertical resolution of 60 m. We further interpolate the temperature data onto the single-shot grid of the cloud phase observations.

3 Quantification of Phase Heterogeneity

Previous work has quantified phase heterogeneity based on the frequency of switches between liquid and ice along an aircraft flight track or on the horizontal extent of single-phase patches within a cloud (Atlas et al., 2021; D'Alessandro et al., 2021). Here we use a metric that is similar in nature but adjusted for use with CALIOP retrievals. We define the *interface density* I [km^{-1}] as the number of interfaces between observations of unlike phase per horizontal kilometer of cloud detected by CALIOP. To compute I, we compare the phase of each cloud observation to the phase of the immediately adjacent observations at the same vertical level. The boundary between two pixels is considered to be a liquid-ice interface only if one of the pixels is liquid and the other is ice (either randomly or horizontally oriented) and only if both phase determinations are of medium or high confidence. Each cloud observation is assigned a value of 0, 1, or 2 equal to the number of liquid-ice interfaces at its horizontal edges. We can then compute I for any subset of observations as

$$I = \frac{(N_1/2 + N_2)}{N_c \cdot \Delta x} \tag{1}$$

where N_1 and N_2 are the number of cloud observations with one and two adjacent interfaces, respectively, and $N_c = N_0 + N_1 + N_2$ is the total number of cloud observations with medium- or high-confidence phase determinations. N_1 is scaled by a factor of 1/2 so that interfaces are not double-counted. Δx is the horizontal resolution of the retrievals (333 m).

When I is large, cloud phase is more heterogeneous: single-phase cloud segments are shorter in length and there is a greater contact area between liquid-only and ice-only patches. Conversely, small I corresponds to large patches of uniform phase. While I can be conceptualized as the inverse of the average length of a single-phase patch, we note that the two quantities are *not* numerically equal because the edge of a cloud is not a liquid-ice interface but nevertheless constitutes the end of a single-phase patch. The two quantities are equal only in the limiting case of a cloud with infinite length.

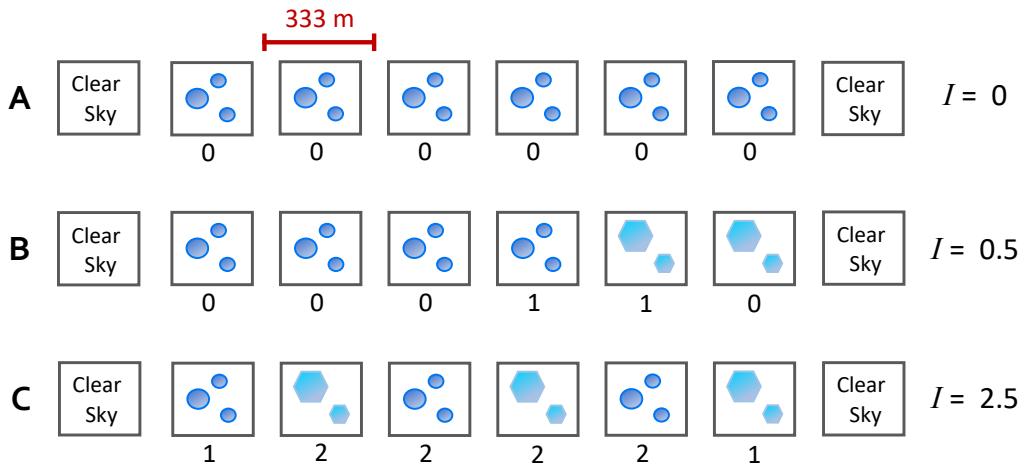

Figure 1. Schematic illustrating the interface density metric, I, used to quantify cloud phase heterogeneity. Each box represents one single-shot lidar profile and its associated high-quality phase retrieval, with the number below indicating the number of liquid-ice interfaces adjacent to the box. Clouds transects A, B, and C all portray clouds that extend for 2-km along the satellite's track. A is single-phase liquid cloud while B and C are mixed-phase clouds with different degrees of heterogeneity. I is computed for each transect following Equation 1.

Figure 1 illustrates I for three schematic cloud transects of equal length. Transect A, an all-liquid cloud with no phase interfaces, represents the most homogeneous possibility (I=0). Transect C, a mixed-phase cloud in which liquid and ice alternate with every observation, represents the most heterogeneous possibility. While I =2.5 km^{-1} for transect C, we note that the theoretical maximum I is 3 km^{-1} (=$1/\Delta x$), which corresponds to an infinitely long cloud with alternating phase retrievals. Transect B, which shows a mixed-phase cloud with one liquid-ice interface, is a compromise between the two extremes.

I is a useful metric for our purposes because it allows us to quantify phase heterogeneity for any subset of cloud observations. Once each pixel has been assigned a value of 0, 1, or 2, the pixels can be binned according to some other variable and I can be computed for each bin following Equation 1. We bin the observations by month, latitude (2.5° bins between 82.5°S and 82.5°N), and temperature (1-°C bins between -40 and 0°C). For each of these bins, we also compute the supercooled liquid cloud fraction (LCF), which is the fraction of cloud observations with medium- or high-quality phase determinations that are classified as liquid.

To understand how the characteristic size of an ice-only patch differs from that of a liquid-only patch, I can also be computed separately for each phase. These quantities will be referred to as I_{liq} and I_{ice} and represent the single-phase contributions to total I:

$$I = \text{LCF} \cdot I_{liq} + \text{ICF} \cdot I_{ice} \tag{2}$$

where ICF is the ice cloud fraction equal to 1−LCF. When computing I_{liq} using Equation 1, N_1 is not the total number of cloud observations with one adjacent liquid-ice interface but the number of *liquid* cloud observations meeting that criteria, and so on for N_2 and N_c. I_{ice} is computed in the same manner but for ice instead of liquid. When I_{liq} is large, liquid cloud observations are relatively likely to be adjacent to ice cloud observations, meaning that liquid-only patches are relatively small; conversely, small I_{liq} corresponds to large liquid-only patches. For a set of cloud observations corresponding to a particular temperature range, time period, and/or latitude, the values of I, I_{liq}, I_{ice}, and LCF provide an informative description of cloud phase composition and heterogeneity.

The heterogeneity metrics described above only reflect horizontal heterogeneity. For our purpose of improving model representation of subgrid-scale heterogeneity, it is appropriate to neglect the vertical dimension. Even within the mixed-phase temperature range, cloud phase depends strongly on temperature (A. Korolev et al., 2017), and we therefore expect vertical phase variability to be modulated primarily by changes in temperature rather than the phase "patchiness" that we hope to characterize. Even if phase heterogeneity were spatially isotropic, it would still be appropriate to neglect subgrid-scale vertical heterogeneity for our purposes, since the horizontal dimension of a GCM grid box is ∼2 orders of magnitude larger than the vertical dimension.

4 Dependence on Temperature and Cloud Phase Composition

We first examine the covariance between temperature, I, and LCF. Figure 2a shows global mean I and LCF as a function of temperature. The LCF curve shows a relatively smooth transition from liquid to ice between 0 and -40°C, in line with previous work (A. Korolev et al., 2017; Cesana et al., 2016). I is lowest at cold temperatures and peaks broadly between -2 and -15°C before decreasing slightly between -4 and 0°C. Maximum heterogeneity occurs at -4°C, where LCF=86% and I=0.17 km^{-1}; this value of I corresponds to one phase interface for every 6 km of cloud observations. The fact that maximum I coincides with high LCF while low I coincides with low LCF means that pockets of ice within majority-liquid clouds are generally smaller than pockets of liquid within majority-ice clouds. This makes sense considering that the WBF process would act to quickly glaciate small pockets of liquid that are surrounded by ice.

Phase heterogeneity can be more fully understood by considering how I_{liq} and I_{ice} vary with cloud phase composition. To do so, we group the month-latitude-temperature bins by LCF (ICF) and compute the mean I_{liq} (I_{ice}) for each group. Results are shown in Figure 2b. At low LCF/ICF, I_{ice} is about twice as large as I_{liq}, meaning that ice tends to exist in much smaller pockets when it is the lesser phase than does liquid when liquid is the lesser phase. It is then inevitable that I_{liq} exceeds I_{ice} at high LCF/ICF, since continuous stretches of liquid are disrupted by the presence of small ice pockets. Conversely, in ice-dominated conditions, liquid patches are larger in size but fewer in number, allowing for long continuous stretches of ice. This is again consistent with what one may expect from WBF thermodynamics: small liquid pockets vanish quickly at very cold temperatures due to rapid WBF glaciation, but liquid within larger pockets can persist because of its greater separation from ice.

5 Spatiotemporal Variability

Having established the strong dependence of I on temperature, we turn now to the spatial and temporal variability of phase heterogeneity. Figure 3 shows zonal monthly mean I as a function of time over the three-year study period for four 10-K temperature bins (data are available in Data Set S1). Statistics are unavailable in the tropics at the coldest temperatures because such temperatures seldom occur below 8.2 km there. Broadly, Figure 3 shows that, within a fixed temperature range, I is generally highest

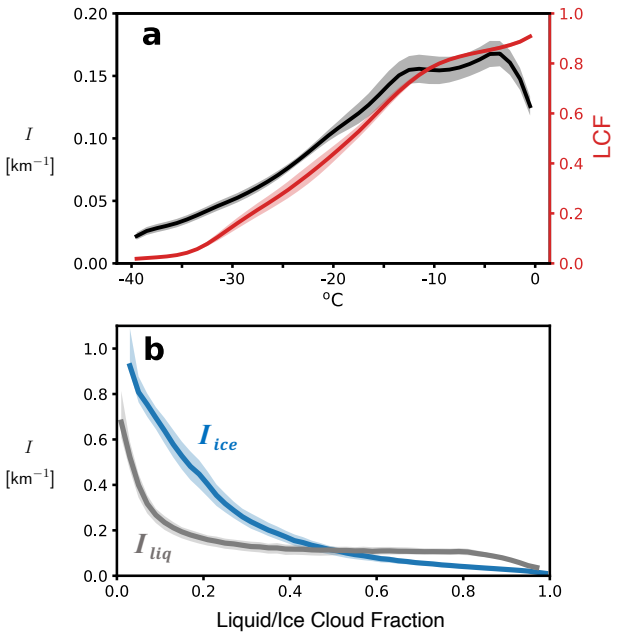

Figure 2. **(a)** Global mean I (black) and LCF (red). Shading indicates 1σ of the monthly global mean values within each temperature bin. **(b)** I_{liq} and I_{ice} as a function of liquid and ice cloud fraction, respectively. Curves show global means computed for LCF/ICF bins with a width of 0.02. Shading shows the 25th and 75th percentiles of the month-latitude-temperature bins within each LCF bin. Statistics only reflect month-latitude-temperature bins with more than 10^4 observations.

in the midlatitudes. For $T > -20°C$, I is greater in the Northern Hemisphere (NH) than in the Southern Hemisphere (SH), with less hemispheric contrast at colder temperatures.

Outside of the tropics, I at some fixed latitude undergoes a clear annual cycle that generally has a larger amplitude in the NH. In the NH, the annual cycle consists of a rather abrupt rise in I followed by a 2-3 month period of enhanced heterogeneity before I declines more gradually. This pattern is discernible within the three warmest temperature bins but not at temperatures below -30°C. The exact timing of peak I varies with latitude but appears to follow seasonal shifts in the storm track. Between 30°-40°N, I is greatest during the boreal winter. The band of enhanced I moves poleward over the course of boreal spring, following the poleward retreat of the storm track (Hoskins & Hodges, 2019).

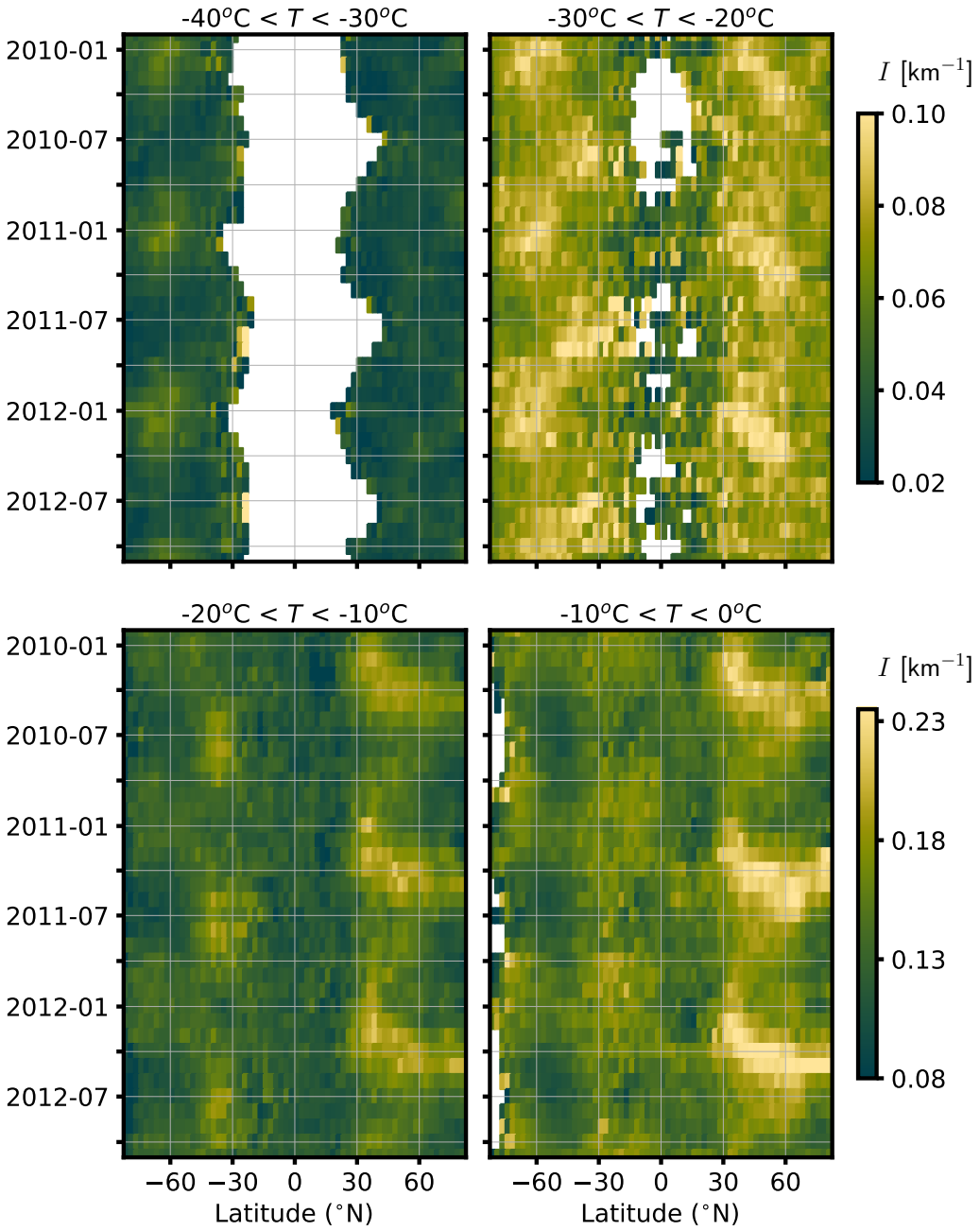

Figure 3. Zonal monthly mean I throughout the three-year study period for four different temperature brackets. Data are only shown for bins containing 10^4 or more cloud phase retrievals. The top two panels use a different color scale than the bottom two panels in order to highlight the variability within each temperature range.

The annual cycle of phase heterogeneity in the SH is similar in some respects to that in the NH but different in others. As in the NH, at 30°-40°S I is greatest during lo-

cal winter, when the storm track is more equatorward than at any other point in the year. Notably, this feature is only seen between -30˚and -10°C and not in the warmest temperature bin. Unlike the NH, there is no clear progression of enhanced I towards the poles over the course of the spring. Poleward of 50°S, I is greatest during summer. Uncovering the shifts in cloud type that are responsible for these seasonal shifts in phase heterogeneity may be a worthwhile endeavor but is beyond our scope here.

It is notable that I is relatively low over the Southern Ocean (SO) region (∼50-70°S) compared to similar latitudes in the NH. This is consistent with the fact that, in some models, biases in LCF and absorbed shortwave radiation are larger over the SO than in the extratropical NH (Trenberth & Fasullo, 2010; Tan et al., 2016; Kay et al., 2016). Lower I over the SO implies relatively little contact area between liquid and ice and thus a reduced potential for widespread WBF glaciation. The failure of models to account for subgrid phase heterogeneity would thus be expected to produce the largest LCF biases where I is low.

The seasonality in phase heterogeneity over the SO is also consistent with expectations from previous modeling studies. Kay et al. (2016) found that SO phase partitioning biases in the CAM5 model were greatest between March and August (see their Figs. 9 and 10). Figure 3 shows that I at 60°S is lowest during this half of the year throughout the entire mixed-phase temperature range. These results underscore the need to incorporate seasonal variability into model representations of subgrid heterogeneity.

6 Discussion

The results shown here show that cloud phase heterogeneity has strong dependencies on temperature, latitude, and time of year. Even at fixed latitude and temperature, I can vary by factor of ∼2 over the course of the year; such variability has important implications for WBF glaciation and should be accounted for in any model implementation of subgrid phase heterogeneity. Figure 4 proposes one relatively simple way of accounting for this variability: mean I is computed for five zonal bands, four seasons, and four 10-$^{\circ}C$ temperature ranges. While these bins are relatively coarse, they capture most of the variability in phase heterogeneity evident in Figure 3. The values shown in Figure 4 are available in Data Set S2.

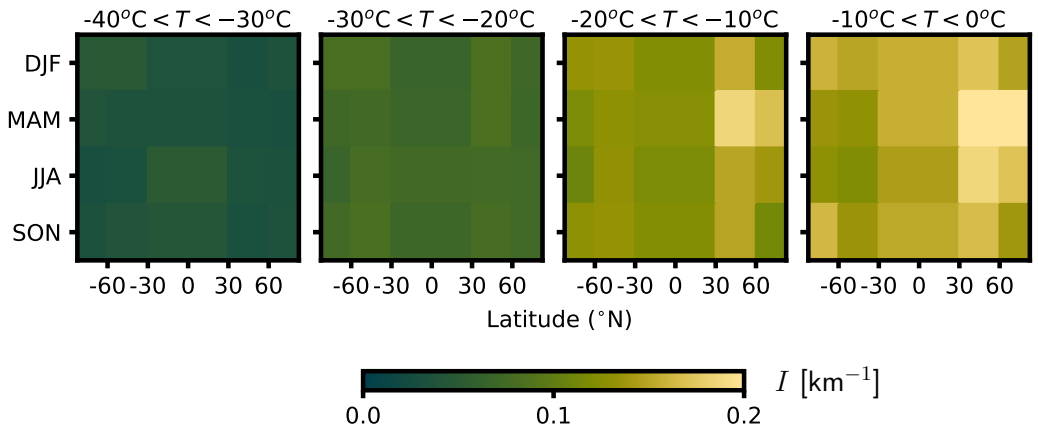

Figure 4. Zonally and seasonally averaged I for four different temperature brackets.

Future work will focus on how to meaningfully convert I to a scaling parameter that can be used to adjust WBF efficiency in models. Such implementation must consider the fact that I is a measure of liquid-ice interface density at a fixed vertical level along a one-dimensional satellite track. Even if vertical phase heterogeneity is to be neglected, I must still be generalized from one horizontal dimension to two. Implementations may vary from model to model due to differences in grid type and WBF parameterizations, and for this reason we leave the details of such implementation for future work.

The use of CALIOP to study phase heterogeneity has several sources of error in addition to the limitation of horizontal resolution discussed in section 1. About 17% of the cloud observations in our study period lacked a high-quality phase determination and were not included in our analysis. Thus, the number of liquid-ice interfaces identified using our methodology is almost certainly an underestimate, not to mention the fact that some of the excluded observations are likely mixed-phase. Another potential source of bias is the fact that the lidar signal attenuates at an optical depth of ∼5 (Winker et al., 2009), which means that our results are skewed to represent conditions near cloud top for optically thick clouds, such as the low marine clouds common over the Southern Ocean. This bias would only affect our results if there is significant vertical variation in cloud phase heterogeneity. Lastly, we draw attention to the source of error discussed in Mace et al. (2021), who demonstrated the difficulty of observing mixed-phase clouds using spaceborne lidar. In particular, they documented the presence of low clouds over the Southern Ocean that are mixed-phase but appear to spaceborne lidar as supercooled liquid

because the layer scattering characteristics are heavily dominated by liquid droplets. The inability of spaceborne lidar to identify the presence of ice in such clouds is an inherent limitation of our methodology.

This paper presents, to our knowledge, the first comprehensive, global assessment of cloud phase heterogeneity using spaceborne satellites. Such an assessment is valuable because it strikes a balance between horizontal resolution and spatiotemporal coverage. While spaceborne lidar cannot be used to study phase heterogeneity on the scale of individual cloud particles, our results show that it is capable of capturing differences in phase heterogeneity on scales much smaller than a GCM grid box. In this way, it offers a useful complement to *in situ* aircraft observations and a good opportunity to improve model representations of cloud phase.

7 Open Research

The CAILOP retrievals used in this study (NASA/LARC/SD/ASDC, 2018a, 2018b) are publicly available at https://search.earthdata.nasa.gov. Phase heterogeneity statistics are provided in Data Set S1.

Acknowledgments

This work was supported by the European Research Council (ERC) through Grant StG 758005.

References

Atlas, R., Mohrmann, J., Finlon, J., Lu, J., Hsiao, I., Wood, R., & Diao, M. (2021, November). The University of Washington Ice–Liquid Discriminator (UWILD) improves single-particle phase classifications of hydrometeors within Southern Ocean clouds using machine learning. *Atmospheric Measurement Techniques*, *14*(11), 7079–7101. doi: 10.5194/amt-14-7079-2021

Avery, M. A., Ryan, R. A., Getzewich, B. J., Vaughan, M. A., Winker, D. M., Hu, Y., ... Verhappen, C. A. (2020, August). CALIOP V4 cloud thermodynamic phase assignment and the impact of near-nadir viewing angles. *Atmospheric Measurement Techniques*, *13*(8), 4539–4563. doi: 10.5194/amt-13-4539-2020

Cesana, G., Chepfer, H., Winker, D., Getzewich, B., Cai, X., Jourdan, O., ... Reverdy, M. (2016). Using in situ airborne measurements to evaluate three

cloud phase products derived from CALIPSO. *Journal of Geophysical Research: Atmospheres*, *121*(10), 5788–5808. doi: 10.1002/2015JD024334

Cesana, G., Waliser, D. E., Jiang, X., & Li, J.-L. F. (2015). Multimodel evaluation of cloud phase transition using satellite and reanalysis data. *Journal of Geophysical Research: Atmospheres*, *120*(15), 7871–7892. doi: 10.1002/2014JD022932

Choi, Y.-S., Ho, C.-H., Park, C.-E., Storelvmo, T., & Tan, I. (2014). Influence of cloud phase composition on climate feedbacks. *Journal of Geophysical Research: Atmospheres*, *119*(7), 3687–3700. doi: 10.1002/2013JD020582

Chylek, P., & Borel, C. (2004). Mixed phase cloud water/ice structure from high spatial resolution satellite data. *Geophysical Research Letters*, *31*(14). doi: 10.1029/2004GL020428

D'Alessandro, J. J., McFarquhar, G. M., Wu, W., Stith, J. L., Jensen, J. B., & Rauber, R. M. (2021). Characterizing the Occurrence and Spatial Heterogeneity of Liquid, Ice, and Mixed Phase Low-Level Clouds Over the Southern Ocean Using in Situ Observations Acquired During SOCRATES. *Journal of Geophysical Research: Atmospheres*, *126*(11), e2020JD034482. doi: 10.1029/2020JD034482

D'Alessandro, J. J., Diao, M., Wu, C., Liu, X., Jensen, J. B., & Stephens, B. B. (2019, May). Cloud Phase and Relative Humidity Distributions over the Southern Ocean in Austral Summer Based on In Situ Observations and CAM5 Simulations. *Journal of Climate*, *32*(10), 2781–2805. doi: 10.1175/JCLI-D-18-0232.1

Field, P. R., Hogan, R. J., Brown, P. R. A., Illingworth, A. J., Choularton, T. W., Kaye, P. H., ... Greenaway, R. (2004). Simultaneous radar and aircraft observations of mixed-phase cloud at the 100 m scale. *Quarterly Journal of the Royal Meteorological Society*, *130*(600), 1877–1904. doi: 10.1256/qj.03.102

Frey, W. R., & Kay, J. E. (2018, April). The influence of extratropical cloud phase and amount feedbacks on climate sensitivity. *Climate Dynamics*, *50*(7), 3097–3116. doi: 10.1007/s00382-017-3796-5

Hoskins, B. J., & Hodges, K. I. (2019, March). The Annual Cycle of Northern Hemisphere Storm Tracks. Part II: Regional Detail. *Journal of Climate*, *32*(6), 1761–1775. doi: 10.1175/JCLI-D-17-0871.1

Hu, Y., Winker, D., Vaughan, M., Lin, B., Omar, A., Trepte, C., ... Kuehn, R. (2009, November). CALIPSO/CALIOP Cloud Phase Discrimination Algorithm. *Journal of Atmospheric and Oceanic Technology*, *26*(11), 2293–2309. doi: 10.1175/2009JTECHA1280.1

Huang, Y., Dong, X., Kay, J. E., Xi, B., & McIlhattan, E. A. (2021, May). The climate response to increased cloud liquid water over the Arctic in CESM1: a sensitivity study of Wegener–Bergeron–Findeisen process. *Climate Dynamics*, *56*(9), 3373–3394. doi: 10.1007/s00382-021-05648-5

Kay, J. E., Bourdages, L., Miller, N. B., Morrison, A., Yettella, V., Chepfer, H., & Eaton, B. (2016). Evaluating and improving cloud phase in the Community Atmosphere Model version 5 using spaceborne lidar observations. *Journal of Geophysical Research: Atmospheres*, *121*(8), 4162–4176. doi: 10.1002/2015JD024699

Komurcu, M., Storelvmo, T., Tan, I., Lohmann, U., Yun, Y., Penner, J. E., ... Takemura, T. (2014). Intercomparison of the cloud water phase among global climate models. *Journal of Geophysical Research: Atmospheres*, *119*(6), 3372–3400. doi: 10.1002/2013JD021119

Korolev, A., McFarquhar, G., Field, P. R., Franklin, C., Lawson, P., Wang, Z., ... Wendisch, M. (2017, January). Mixed-Phase Clouds: Progress and Challenges. *Meteorological Monographs*, *58*(1), 5.1–5.50. doi: 10.1175/AMSMONOGRAPHS-D-17-0001.1

Korolev, A. V., Isaac, G. A., Cober, S. G., Strapp, J. W., & Hallett, J. (2003). Microphysical characterization of mixed-phase clouds. *Quarterly Journal of the Royal Meteorological Society*, *129*(587), 39–65. doi: 10.1256/qj.01.204

Mace, G. G., Protat, A., & Benson, S. (2021). Mixed-Phase Clouds Over the Southern Ocean as Observed From Satellite and Surface Based Lidar and Radar. *Journal of Geophysical Research: Atmospheres*, *126*(16), e2021JD034569. doi: 10.1029/2021JD034569

McIlhattan, E. A., L'Ecuyer, T. S., & Miller, N. B. (2017, June). Observational Evidence Linking Arctic Supercooled Liquid Cloud Biases in CESM to Snowfall Processes. *Journal of Climate*, *30*(12), 4477–4495. doi: 10.1175/JCLI-D-16-0666.1

Mitchell, J. F. B., Senior, C. A., & Ingram, W. J. (1989, September). C02

and climate: a missing feedback? *Nature*, *341*(6238), 132–134. doi: 10.1038/341132a0

NASA/LARC/SD/ASDC. (2018a, October). *CALIPSO Lidar Level 2 Cloud Profile, V4-20.* NASA Langley Atmospheric Science Data Center DAAC. Retrieved from `https://doi.org/10.5067/CALIOP/CALIPSO/LID_L2_05KMCPRO-STANDARD-V4-20`

NASA/LARC/SD/ASDC. (2018b, October). *CALIPSO Lidar Level 2 Vertical Feature Mask (VFM), V4-20.* NASA Langley Atmospheric Science Data Center DAAC. Retrieved from `https://doi.org/10.5067/CALIOP/CALIPSO/LID_L2_VFM-STANDARD-V4-20`

Storelvmo, T., & Tan, I. (2015). The Wegener-Bergeron-Findeisen process - Its discovery and vital importance for weather and climate. *Meteorologische Zeitschrift*, *24*(4), 455–461. doi: 10.1127/METZ/2015/0626

Storelvmo, T., Tan, I., & Korolev, A. V. (2015, December). Cloud Phase Changes Induced by CO2 Warming—a Powerful yet Poorly Constrained Cloud-Climate Feedback. *Current Climate Change Reports*, *1*(4), 288–296. doi: 10.1007/s40641-015-0026-2

Tan, I., & Storelvmo, T. (2016, February). Sensitivity Study on the Influence of Cloud Microphysical Parameters on Mixed-Phase Cloud Thermodynamic Phase Partitioning in CAM5. *Journal of the Atmospheric Sciences*, *73*(2), 709–728. doi: 10.1175/JAS-D-15-0152.1

Tan, I., Storelvmo, T., & Zelinka, M. D. (2016, April). Observational constraints on mixed-phase clouds imply higher climate sensitivity. *Science*, *352*(6282), 224–227. doi: 10.1126/science.aad5300

Thompson, D. R., Kahn, B. H., Green, R. O., Chien, S. A., Middleton, E. M., & Tran, D. Q. (2018, February). Global spectroscopic survey of cloud thermodynamic phase at high spatial resolution, 2005–2015. *Atmospheric Measurement Techniques*, *11*(2), 1019–1030. doi: 10.5194/amt-11-1019-2018

Trenberth, K. E., & Fasullo, J. T. (2010, January). Simulation of Present-Day and Twenty-First-Century Energy Budgets of the Southern Oceans. *Journal of Climate*, *23*(2), 440–454. doi: 10.1175/2009JCLI3152.1

Tsushima, Y., Emori, S., Ogura, T., Kimoto, M., Webb, M. J., Williams, K. D., ... Andronova, N. (2006, August). Importance of the mixed-phase cloud distri-

bution in the control climate for assessing the response of clouds to carbon dioxide increase: a multi-model study. *Climate Dynamics*, *27*(2), 113–126. doi: 10.1007/s00382-006-0127-7

Winker, D. M., Vaughan, M. A., Omar, A., Hu, Y., Powell, K. A., Liu, Z., ... Young, S. A. (2009, November). Overview of the CALIPSO Mission and CALIOP Data Processing Algorithms. *Journal of Atmospheric and Oceanic Technology*, *26*(11), 2310–2323. doi: 10.1175/2009JTECHA1281.1

Zelinka, M. D., Myers, T. A., McCoy, D. T., Po-Chedley, S., Caldwell, P. M., Ceppi, P., ... Taylor, K. E. (2020, January). Causes of Higher Climate Sensitivity in CMIP6 Models. *Geophysical Research Letters*, *47*(1). doi: 10.1029/2019GL085782

Zhang, M., Liu, X., Diao, M., D'Alessandro, J. J., Wang, Y., Wu, C., ... Xie, S. (2019). Impacts of Representing Heterogeneous Distribution of Cloud Liquid and Ice on Phase Partitioning of Arctic Mixed-Phase Clouds with NCAR CAM5. *Journal of Geophysical Research: Atmospheres*, *124*(23), 13071–13090. doi: 10.1029/2019JD030502

Figure 1.

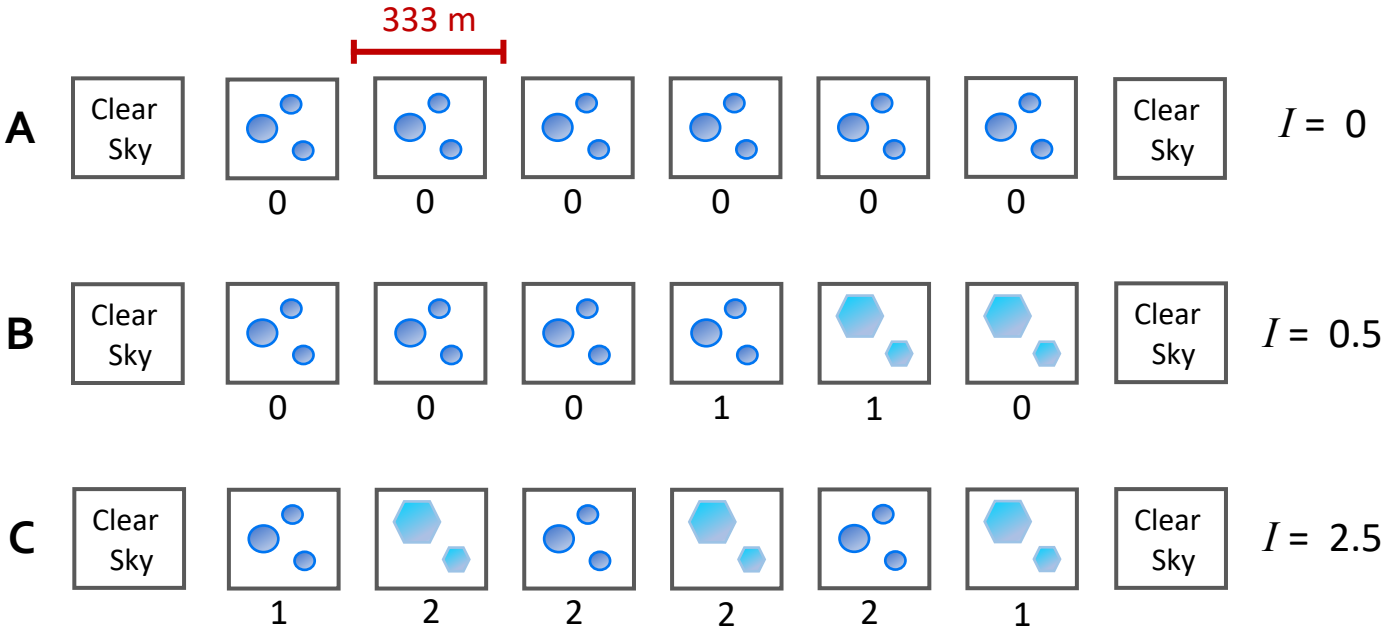
333 m
A
Clear Sky
0
0
0
0
0
0
Clear Sky
I = 0
B
Clear Sky
0
0
0
1
1
0
Clear Sky
I = 0.5
C
Clear Sky
1
2
2
2
2
1
Clear Sky
I = 2.5

Figure 2.

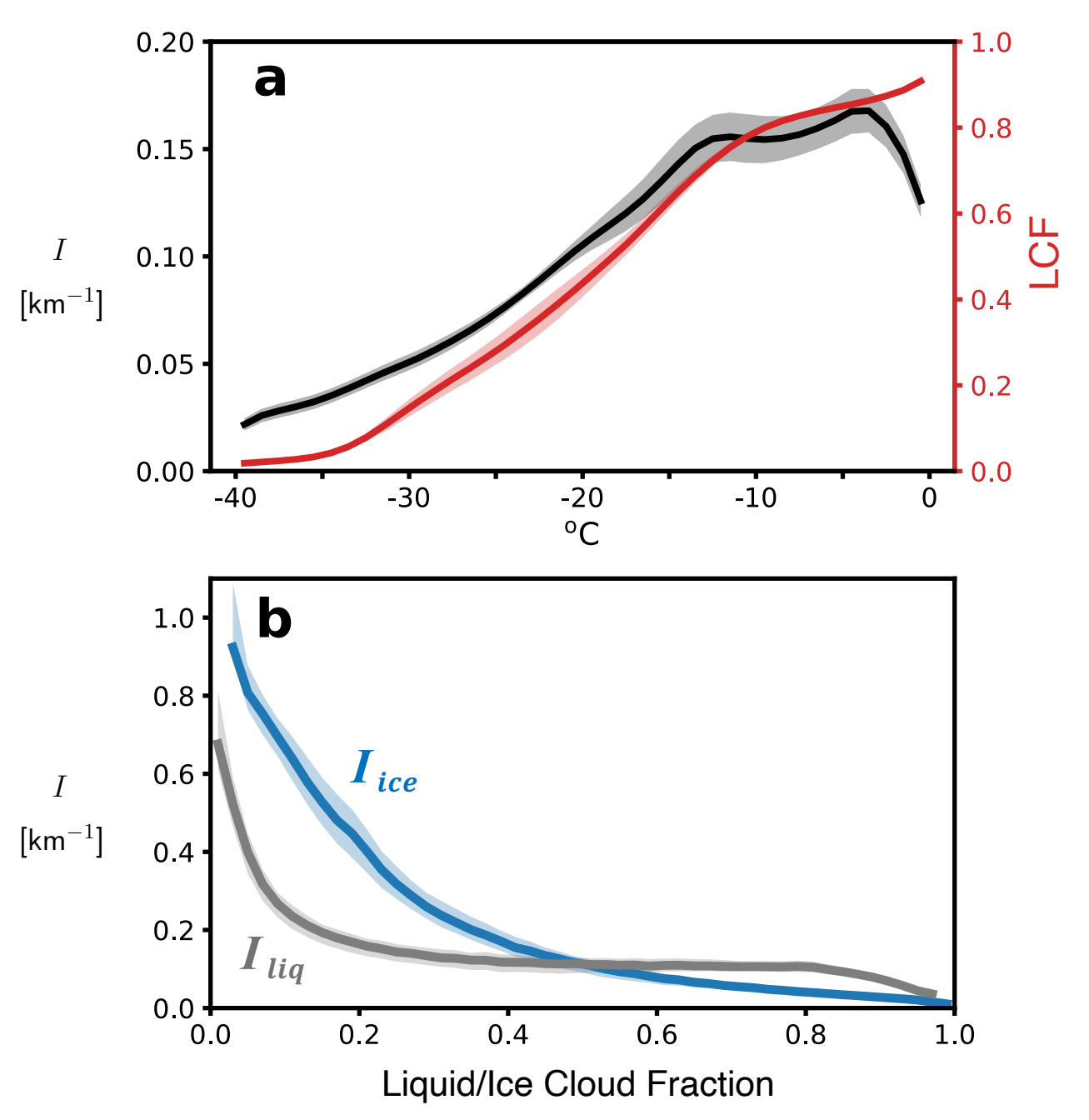
a
0.20
0.15
0.10
0.05
0.00
I
[km^{-1}]
1.0
0.8
0.6
0.4
0.2
0.0
LCF
-40
-30
-20
-10
0
°C
b
1.0
0.8
0.6
0.4
0.2
0.0
I
[km^{-1}]
I_{ice}
I_{liq}
0.0
0.2
0.4
0.6
0.8
1.0
Liquid/Ice Cloud Fraction

Figure 3.

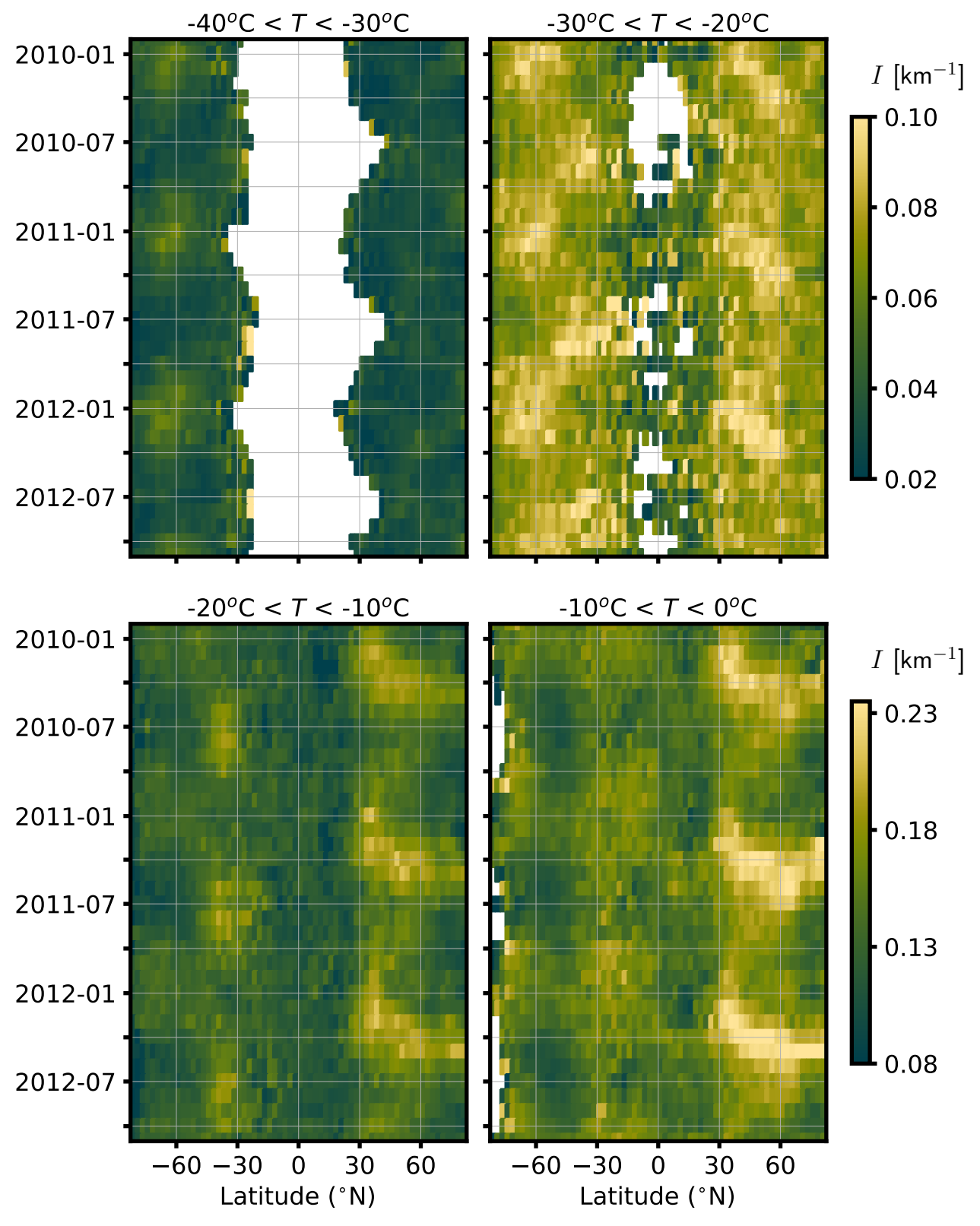
-40°C < T < -30°C
-30°C < T < -20°C
-20°C < T < -10°C
-10°C < T < 0°C
2010-01
2010-07
2011-01
2011-07
2012-01
2012-07
I [km⁻¹]
0.10
0.08
0.06
0.04
0.02
I [km⁻¹]
0.23
0.18
0.13
0.08
−60 −30 0 30 60
Latitude (°N)
−60 −30 0 30 60
Latitude (°N)

Figure 4.

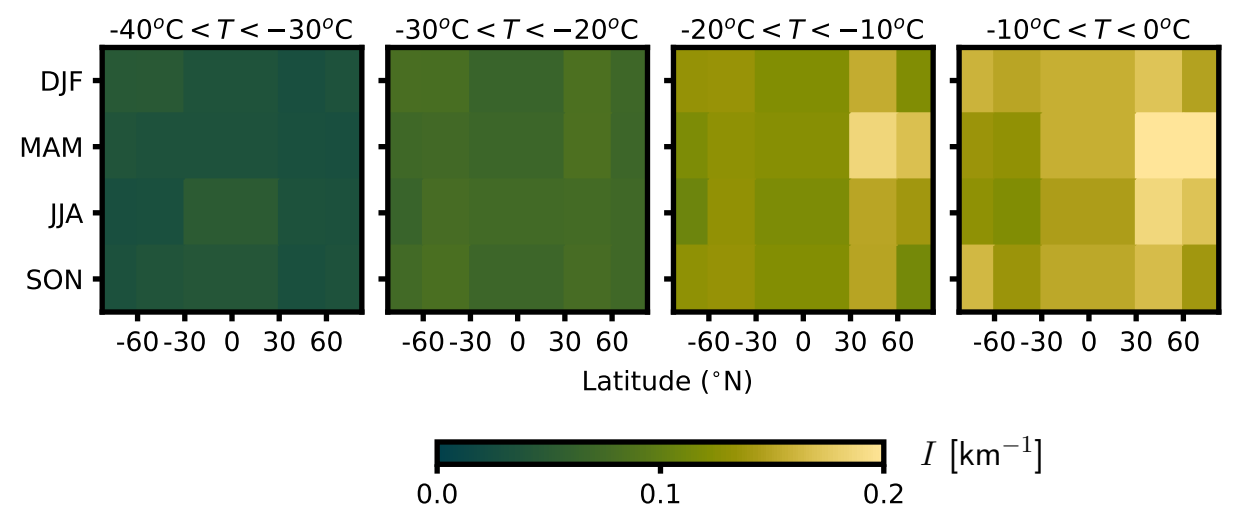
-40°C < T < −30°C
-30°C < T < −20°C
-20°C < T < −10°C
-10°C < T < 0°C
DJF
MAM
JJA
SON
-60 -30 0 30 60
Latitude (°N)
I [km⁻¹]
0.0
0.1
0.2